Journal of Materials Chemistry A

Accepted Manuscript

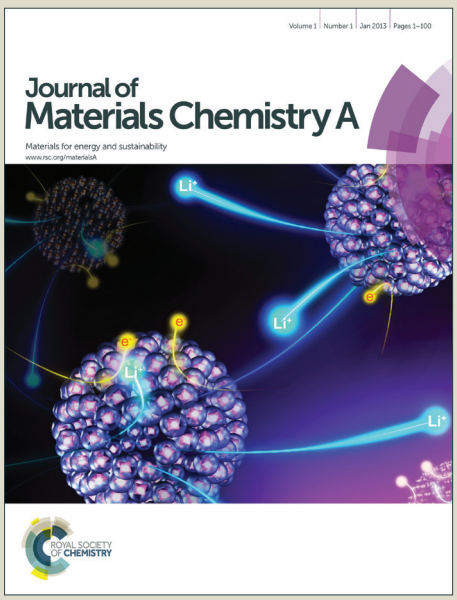

ROYAL SOCIETY OF CHEMISTRY

www.rsc.org/materialsA

Journal Name

RSCPublishing

ARTICLE

Crystal structure and *in situ* decomposition of $Eu(BH_4)_2$ and $Sm(BH_4)_2$

Cite this: DOI: 10.1039/xoxxoooooox

Terry D. Humphries,[a,b] Morten B. Ley,[c] Christoph Frommen,[a] Keelie T. Munroe,[c] Torben R. Jensen[c] and Bjørn C. Hauback[a]*

Received ooth January 2012,
Accepted ooth January 2012

DOI: 10.1039/xoxxoooooox

www.rsc.org/

Synthesis of halide free rare earth metal (*RE*) borohydride complexes is demonstrated by the metathesis reaction of trivalent *RE* metal chlorides and $LiBH_4$ in ethereal solution, combined with solvent extraction using dimethyl sulfide. The crystal structures of $Eu(BH_4)_2$ and $Sm(BH_4)_2$ are orthorhombic (space group *Pbcn*) and are shown to be related to the structure of $Sr(BH_4)_2$ by Rietveld refinement. Further, the thermal decomposition of these materials has been studied by *in situ* synchrotron radiation powder X-ray diffraction, differential scanning calorimetry, thermogravimetric analysis, mass spectrometry and Sieverts measurements. The decomposition pathway of these solvent extracted materials has been compared against materials prepared by mechano-chemistry, the process of which is simplified by the absence of chloride impurities.

Introduction

The research and development of renewable energies, alternative fuels and new methods for energy storage and conversion have become part of many countries' political and scientific discourse. Hydrogen is the lightest element of all with the highest gravimetric energy density, and is considered one of the most promising options to store the extreme amounts of energy that must be harvested to level out the strongly fluctuating renewable sources such as solar and wind energy.[1]

A host of rare earth metal (*RE*) borohydrides have recently been identified and structurally investigated, some of which may act as hydrogen storage materials or new multifunctional materials.[2-10] The hydrogen content of rare earth metal borohydrides (*e.g.* $\rho_m(Y(BH_4)_3)$ = 9.0 wt% H) is highly acceptable in regards to more established materials such as $NaAlH_4$ (7.5 wt% H), and initial studies have determined that thermal decomposition initiates at moderate temperatures (190 °C) producing high purity H_2.[11] In addition, their optical and magnetic properties and most recently their electrochemical properties have been investigated for new potential applications.[12-15] The new series of isostructural materials, $LiM(BH_4)_3Cl$ (*M* = La, Ce, Pr, Nd, Sm, or Gd), store hydrogen and are simultaneous fast lithium ion conductors.[2-6] These materials have a fascinating structure, containing isolated tetranuclear anionic clusters (e.g. $[Ce_4Cl_4(BH_4)_{12}]^{4-}$), with a distorted cubane Ce_4Cl_4 core and are charge-balanced by disordered Li^+ cations occupying 2/3 of the available positions.

The synthesis of the transition metal (*TM*) and *RE* borohydrides has traditionally been via mechano-chemically facilitated metathesis reactions using alkali metal borohydrides (Li, Na, K) and metal chlorides.[2, 8, 16] This usually leads to the formation of mixed-metal and often anion-substituted borohydrides such as $NaSc(BH_4)_4$, $LiCe(BH_4)_3Cl$ or solid solutions such as $Na(BH_4)_xCl_{1-x}$.[2, 5, 17, 18] The halide side-product is often difficult to remove and may hinder the reversible hydrogenation of the metal borohydride due to formation of ternary chlorides. The solvent mediated synthesis of borohydrides has been employed for over five decades and allows for the production of borohydrides free from alkali metal chloride impurities.[19] Using O-donor solvents such as THF often leads to the formation of strongly coordinating solvent adducts, where the solvent is difficult to remove without decomposition of the product.[20, 21]

Recent publications by Olsen et al.[3, 6] and Gennari[7] detail the solvent free borohydride complexes of La, Ce, Pr, Nd, Sm, Eu, Gd, Tb, Er, Yb or Lu by *in situ* X-ray powder diffraction, thermal analysis and vibrational spectroscopy. Unfortunately, these compounds contain lithium and chloride impurities, but within these studies the majority of their crystal structures were determined and a significant trend was observed. La, Ce, Pr and Nd form $LiRE(BH_4)_3Cl$ compounds, which crystallise in the cubic space group *I*−*43m*; Sm, Gd, Tb, Er and Yb form $RE(BH_4)_3$ compounds crystallising in the cubic space group *Pa*−*3*, with a possible polymorphic transition to a higher symmetry space group, *Fm*−*3m*. The smaller *RE*-elements Yb and Lu form tetrahedral $[RE(BH_4)_4]^-$ anionic complexes stabilised by Li^+ cations crystallising in the tetragonal space group *P*−*42c*. Additionally, Sm and Gd also exhibit a transition to the $LiRE(BH_4)_3Cl$ polymorph observed for the largest lanthanides. Samarium, Sm^{3+}, in $LiSm(BH_4)_3Cl$ is reduced to $Sm(BH_4)_2$ upon heating, which exhibits an orthorhombic structure in the space group *Pbcn*.[6]

In this study, $Eu(BH_4)_2$ and $Sm(BH_4)_2$ have been synthesised by solvent techniques and their crystal structures refined by the Rietveld method. Further, the thermal decomposition of these materials has been studied by *in situ* synchrotron radiation powder X-ray diffraction (SR-PXD), differential scanning calorimetry (DSC), thermogravimetric analysis (TGA), temperature-programmed desorption mass spectrometry (TPD-MS), and Sieverts measurements. The decomposition pathway of these solvent extracted materials has been compared against materials prepared by mechano-milling. Infrared spectroscopy (IR) and reversibility studies have also been conducted.

Experimental

$LiBH_4$ (95%), $EuCl_3$ (99.99%), $EuCl_2$ (99.99%), $SmCl_3$ (99.99%), dimethyl sulphide (Me_2S) (anhydrous, 99.9%) and diethyl ether (Et_2O) (anhydrous, >99.7%) were purchased from Sigma-Aldrich and used as received, unless otherwise stated. Preparation and manipulation were conducted using standard Schlenk or dry-box techniques *in vacuo* or under an atmosphere of purified N_2 or Ar (H_2O and O_2 < 1 ppm).

$LiBH_4$, $EuCl_3$ and $SmCl_3$ were individually activated using a Fritsch Pulverisette 4 planetary mill under inert conditions (argon atmosphere), utilising an 80 mL tungsten carbide vial with tungsten carbide balls (o.d. 10 mm). A ball to powder ratio of 32:1 was employed. The sample was ball-milled (BM) for 5 min with a 2 min pause for 10 repetitions, at a speed of 200 rpm.

The *RE* metal chloride and $LiBH_4$ were mixed in appropriate ratios, as described in Table 1, to which Et_2O was added and agitated overnight. The Et_2O was removed *in vacuo*, before adding Me_2S and leaving this suspension overnight. The resultant mixture was filtered using standard solvent-based extraction techniques.[22] An overview of samples S1-4 and their specific syntheses are described in the Electronic Supporting Information (ESI)†.

Table 1. Composition of the investigated samples, products obtained and temperature of $RE(BH_4)_2$ phase transition to amorphous state.

Sample	Reactants	Method	Products	$RE(BH_4)_2$ Transitional Temperature (°C)[a]
S1	$EuCl_3$-$LiBH_4$ (1:3)	Solvent	$Eu(BH_4)_2{\cdot}xMe_2S$	185
S2	$EuCl_3$-$LiBH_4$ (1:6)	BM/ solvent	$Eu(BH_4)_2{\cdot}xMe_2S$	165
S3	$EuCl_2$-$LiBH_4$ (1:2)	BM	$Eu(BH_4)_2$, LiCl	295
S4	$SmCl_3$-$LiBH_4$ (1:3)	Solvent	$Sm(BH_4)_2{\cdot}xMe_2S$	335

[a]Temperature at which the crystalline $RE(BH_4)_2$ compounds become amorphous as determined by SR-PXD.

Laboratory Structural Characterisation

All samples were initially investigated using laboratory powder X-ray diffraction (PXD) to identify the reaction products and estimate the crystallinity of the samples. PXD measurements were performed in Debye−Scherrer transmission geometry using a Stoe diffractometer equipped with a curved Ge(111) monochromator (Cu $K\alpha_1$ radiation, λ = 1.54060 Å) and a curved position-sensitive detector. Data were collected at room temperature (RT) in the 2θ-range 4 to 127°. All air-sensitive samples were mounted in a glovebox in 0.5 mm glass capillaries sealed with glue.

FT-IR spectra were measured using a Nicolet 380 Avatar Fourier transform infrared spectrometer in transmission mode. The samples were shortly exposed to air when mounted in the spectrometer. FT-IR data and interpretation are included in the ESI†.

In situ SR-PXD Decomposition Studies

In situ time-resolved SR-PXD data for S1 and S2 were collected at beam line P.02.1 at the Petra III, DESY in Hamburg, Germany with a PerkinElmer PXD1621 (2048 × 2048 pixels, 200 μm^2) detector system and wavelength of λ = 0.2072 Å, with exposure times of 10 s. Additional *in situ* SR-PXD experiments were conducted for S1 and S2 at beam line I711, MAX II, MAX IV laboratories, Lund, Sweden. Data were collected using a MAR165 CCD detector system and a wavelength of 0.9924 Å. The CCD camera exposure time was 30 s. The *in situ* sample cell used at P.02.1 and I711 is specially developed for gas/solid reaction studies and allows high pressure and temperature to be applied. The powdered samples were mounted in a sapphire (Al_2O_3) single-crystal tube (o.d. 1.09 mm, i.d. 0.79 mm) in an argon-filled glovebox $p(O_2, H_2O)$ <1 ppm.[23] During the variable-temperature experiments, samples were heated from RT to 300 or 500 °C at a heating rate of 5 °C/min. The temperature was controlled with a thermocouple placed in the sapphire tube in contact with the sample.[24]

SR-PXD data for S3 and S4 were collected at the Swiss-Norwegian Beamlines (SNBL) at the European Synchrotron Radiation Facility (ESRF) in Grenoble, France. A glass capillary (o.d. 0.5 mm) containing the sample was heated from RT to 500 °C at a rate of 5 °C/min, while SR-PXD data were collected. The temperature was controlled with a Cyberstar hot air blower. The two-dimensional SR-PXD patterns (λ = 0.50528 Å) were collected during absorption using a fast pixel detector (Pilatus 2M, Dectris) with an exposure time of 30 s. The capillary was rotated 30° during exposure to improve the powder averaging.

All obtained raw images were transformed to 2D-powder patterns using the FIT2D program[25] and calibration measurements of the standard NIST LaB_6 sample, masking diffraction spots from the single-crystal sapphire sample holder. Uncertainties of the integrated intensities were calculated at each 2θ-point by applying Poisson statistics to the intensity data, considering the geometry of the detector.

Structural Solution of $Eu(BH_4)_2$ and $Sm(BH_4)_2$

The SR-PXD patterns with the highest intensities of the anticipated $RE(BH_4)_2$ compounds were selected for indexing and structure solution. As such, the data collected at 161 °C for S1 and at 225 °C for S4 were chosen. The PXD patterns of both compounds have a clear resemblance to the pattern observed

for $Sr(BH_4)_2$.[26] Hence, structure refinement was performed in the orthorhombic space group *Pbcn,* using atomic coordinates from $Sr(BH_4)_2$. The cell parameters for both compounds are described in Table 2. Powder indexing was performed with the program DICVOL.[27] Structural refinement using the Rietveld method was performed using the GSAS[28] software package, with the graphical interface EXPGUI.[29] The BH_4^- tetrahedral units were treated as semi-rigid bodies and restraints placed on the B−H and H−H distances, at 1.2(±0.1) Å and 1.95(±0.1) Å, respectively. The orientation of the H atoms around the B centre were then refined. A common atomic displacement parameter, U_{iso}, was refined for all B and H atoms. The background was in each case modelled by a Shifted Chebyschev polynomial consisting of 36 points. A Thomson-Cox-Hastings pseudo-Voigt profile function was selected for the global refinement. Unit cell parameters, zero-point, overall scale factors, peak shape mixing parameters, three Gaussian profile parameters (U,V,W) and two Lorentzian profile parameters (X, Y) were refined for both data sets.

Thermal Analysis

Samples S1-4 were studied by simultaneous thermogravimetric analysis (TGA), differential scanning Calorimetry (DSC) and mass spectrometry (MS) using a Netzsch STA449C connected to a Netzsch QMS403C mass spectrometer equipped with a Channeltron detector capable of multi ion detection. The transfer line was heated at 300 °C. Samples were loaded in Al crucibles and heated from RT to 500 °C ($\Delta T/\Delta t$ = 5 °C/min) under Ar flow (60 mL/min).

The hydrogen release and uptake of S1 and S3 (where S3 was previously annealed at 250 °C for 45 min at 100 bar H_2) were studied using Sieverts measurements in a PCTPro 2000 apparatus.[30, 31] Three desorption and absorption cycles were measured for ca. 100 mg of material. Hydrogen desorption data were collected during heating from RT to 450 °C ($\Delta T/\Delta t$ = 3 °C/min) with a back pressure of $p(H_2)$ = 1 bar. Hydrogen absorption measurements were performed at 400 °C and $p(H_2)$ = 100 bar for 8 h. Following the third absorption measurement, all samples were studied using FT-IR and PXD.

Table 2. Crystallographic data for $Eu(BH_4)_2$ (S1) and $Sm(BH_4)_2$ (S4) obtained by Rietveld refinement of SR-PXD data. A common U_{iso} was refined for all B and H atoms. Estimated standard deviations are given in parentheses.

Data					
Chemical formula			Eu B_2 H_8		Sm B_2 H_8
M **(g/mol)**			181.64		180.08
Gravimetric H content (wt%)			4.44		4.48
Crystal system			Orthorhombic		Orthorhombic
Space group			*Pbcn* (60)		*Pbcn* (60)
Unit cell					
a **(Å)**			6.90343(16)		6.97129(14)
b **(Å)**			8.37272(18)		8.43870(17)
c **(Å)**			7.48321(16)		7.56841(14)
Volume (Å^3)			432.533(10)		445.239(9)
Temperature (°C)			161		225
Z			4		4
Density (g/cm^{-3})			2.790		2.686
R_p			1.28		1.84
wR_p			2.17		2.85
Atom	**Wyckoff position**	***x/a***	***y/b***	***z/c***	U_{iso} **(10^{-2} Å^2)**
Eu	4*c*	0.0	0.15042(20)	0.25	3.54(7)
B	8*d*	0.2459(21)	0.3837(31)	0.4335(21)	3.1(8)
H1	8*d*	0.327(11)	0.280(8)	0.352(11)	3.1(8)
H2	8*d*	0.138(11)	0.325(10)	0.540(10)	3.1(8)
H3	8*d*	0.155(12)	0.465(9)	0.332(11)	3.1(8)
H4	8*d*	0.363(10)	0.464(9)	0.509(13)	3.1(8)
Sm	4*c*	0.0	0.15216(!4)	0.25	2.85(3)
B	8*d*	0.2544(14)	0.3710(18)	0.4218(14)	0.3(5)
H1	8*d*	0.384(4)	0.292(4)	0.369(6)	0.3(5)
H2	8*d*	0.153(6)	0.292(5)	0.514(7)	0.3(5)
H3	8*d*	0.164(7)	0.421(6)	0.300(4)	0.3(5)
H4	8*d*	0.316(6)	0.479(5)	0.506(7)	0.3(5)

Results

Crystal Structure of $Eu(BH_4)_2$ (S1) and $Sm(BH_4)_2$ (S4)

At 161 °C, only one crystalline compound is present in the sample S1 (Fig. 1a), which was indexed to an orthorhombic space group *Pbcn* (no. 60) using DICVOL06[32] (Table 2). The unit cell parameters of $Eu(BH_4)_2$ were determined to be a = 6.90343(16), b = 8.37272(18) and c = 7.48321(16) Å, which contains 4 Eu atoms and 8 BH_4^- tetrahedral units occupying a 4*c* special position and an 8*d* general position, respectively. Since no RT data for this compound was available, the *in situ* SR- PXD data were used in the structural refinement using the Rietveld method.

The structure of $Eu(BH_4)_2$ can be described by Eu-$(BH_4)_6$ octahedra

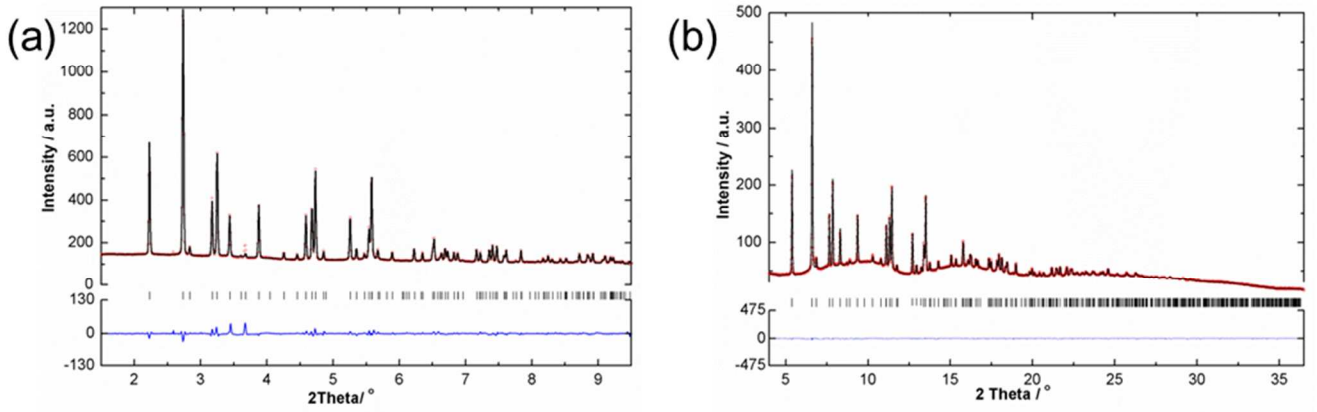

Fig. 1. Rietveld refinement and difference plots for SR-PXD data for (a) $Eu(BH_4)_2$ (S1) collected at 161 °C of (λ = 0.2072 Å) and (b) $Sm(BH_4)_2$ (S4) collected at 225 °C (λ = 0.5053 Å).

Journal Name RSCPublishing

ARTICLE

Table 3. Selected interatomic bond distances (Å) and angles (°) for $Eu(BH_4)_2$ and $Sm(BH_4)_2$ obtained from SR-PXD data. Estimated standard deviations in parentheses.

Atoms (count)	*d* (Å)	Atoms (count)	*d* (Å)
Eu−B (x2)	2.929(20)	Sm−B (x3)	2.872(13)
Eu−B (x2)	3.155(21)	Sm−B (x3)	3.023(10)
Eu−B (x2)	2.961(15)	Sm−H4 (x2)	2.51(6)
Eu−H4 (x2)	2.25(8)	B−H1 (x1)	1.1950(18)
B−H1 (x1)	1.1953(30)	B−H2 (x1)	1.1955(18)
B−H2 (x1)	1.1955(30)	B−H3 (x2)	1.1953(18)
B−H3 (x1)	1.1953(30)		
B−H4 (x1)	1.1951(30)		
Atoms	**Angle (°)**	**Atoms**	**Angle (°)**
Eu−B−Eu	130.8(9)	Sm−B−Sm	132.9(5)
Eu−Eu−Eu	112.10(5)	H1−B−H2	109.48(20)
H1−B−H2	109.52(27)	H1−B−H3	109.48(20)
H1−B−H3	109.51(27)	H1−B−H4	109.54(20)
H1−B−H4	109.45 (27)	B−Sm−B	91.1(3)
B−Eu−B	95.5(4)	B−Sm−B	93.7(3)
B−Eu−B	91.9(4)	B−Sm−B	172.6(4)
B−Eu−B	96.4(9)		
B−Eu−B	168.9(7)		
B−Eu−B	176.7(6)		

sharing edges with two other octahedra at an angle of 112.10(5)° (Fig. 2a), and thus building chains in the *c*-direction (Fig. 2b). Each chain of octahedra is connected via corner sharing to four others. The octahedral environment of BH_4 units around Eu is distorted with *trans* angles of 168.9(7) and 176.7(6)° and Eu−B distances of 2.929(20), 2.961(15) and 3.155(21) Å. Each BH_4^- unit is surrounded by three Eu atoms in a distorted trigonal planar environment (Fig. 2c), where the Eu−B−Eu angle in the edge sharing octahedra is 95.5(4)°. Selected interatomic distances and angles can be found in Table 3.

The structure of $Sm(BH_4)_2$ has previously been reported by Olsen et al. and is identical to that of $Eu(BH_4)_2$[6] and $Sr(BH_4)_2$,[26] albeit an expansion of the unit cell volume incurred by the increased ionic radius of Sm compared to Eu. The ionic radius of Sr^{2+} (r = 1.32 Å), Sm^{2+} (r = 1.36 Å) and Eu^{2+} (r = 1.31 Å) may explain the fact that the corresponding metal borohydrides are isostructural. Crystallographic data and selected interatomic distances and angles for $Sm(BH_4)_2$ extracted by Rietveld refinement of SR-PXD data measured at T = 225 °C can be found in Tables 2 and 3.

The structures and crystal packing of $Sm(BH_4)_4$ and $Eu(BH_4)_4$ are virtually identical, with the only difference being an elongation of the average *RE*−B bond distance from 2.948(12) Å to 3.015(19) Å for Sm and Eu, respectively, and a slightly decreased *RE*−B−*RE* bond angle, i.e. Sm−B−Sm is 132.9(5)°, while Eu−B−Eu is 130.8(9)°.

Thermal Decomposition of $EuCl_3 + 3LiBH_4$ synthesised in Me_2S (S1)

The thermal decomposition of $Eu(BH_4)_2$, S1 (Table 1), was observed by *in situ* SR-PXD, PCT, DSC, TGA and the gas released was analysed by MS, the results of which are illustrated in Figs. 3 and 4. The initial diffraction pattern, collected at RT, is a crystalline solvent-containing compound, with possible composition $Eu(BH_4)_2{\cdot}xMe_2S$, although poor diffracted intensity impedes structural analysis. There is no trace of the reactants $EuCl_3$ or $LiBH_4$ or the by-product LiCl. TGA (Fig. 4a(i)) indicates a mass loss of ~27 wt% in the temperature range RT to 205 °C in accord with one solvent molecule per formula unit, i.e. $Eu(BH_4)_2{\cdot}Me_2S$ (calculated mass loss of 23.9 wt%). The release of Me_2S was also identified by MS, Fig. 4a(iv) in the temperature range 65 to 300 °C. A small desorption of B_2H_6 was also observed between 114 and 124 °C, (along with a small amount of H_2)[33] again between 190 and 269

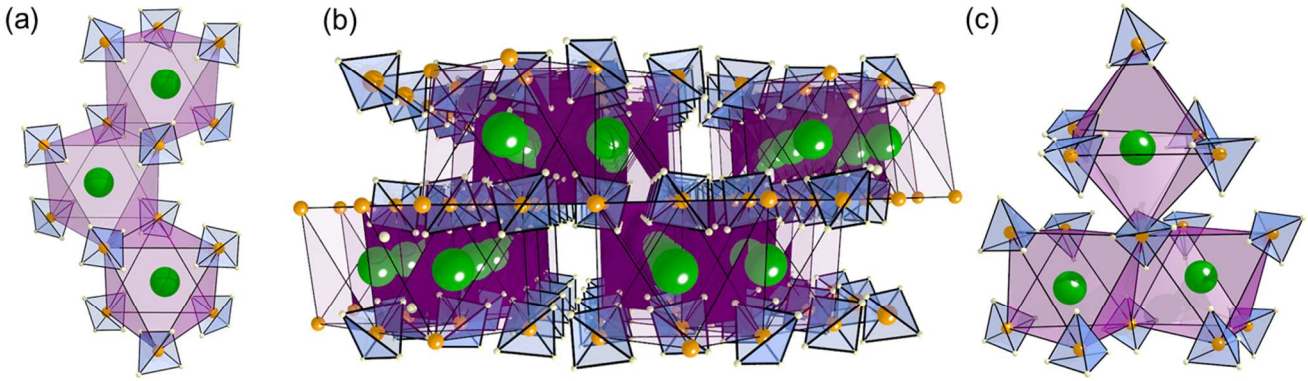

Fig. 2. Representative views of $RE(BH_4)_2$ (*RE* = Eu, Sm). (a) *RE*-$(BH_4)_6$ octahedral units along the chain in *c;* (b) Viewed along the *c*-axis; (c) *RE*-$(BH_4)_6$ octahedral units with a central BH_4^- unit surrounded by 3*RE* atoms in a distorted trigonal planar environment. *RE* atoms as green spheres, BH_4^- tetrahedra represented with blue faces and Eu-$(BH_4)_6$ octahedra represented with purple faces.

Journal Name RSCPublishing

ARTICLE

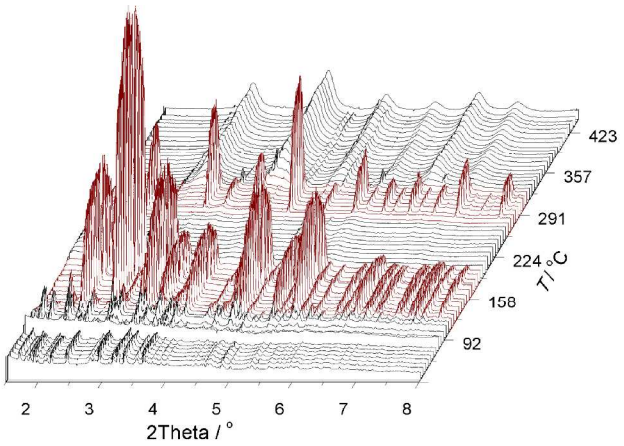

Fig. 3. *In situ* SR-PXD data of $Eu(BH_4)_2$ S1 ($\Delta T/\Delta t$ = 5°C/min, λ = 0.2072 Å).

°C explaining the constant mass loss throughout the TGA experiment (Fig. 4a(v)).

At ~105 °C, diffraction from crystalline single-phase $Eu(BH_4)_2$ emerges as observed by SR-PXD (Fig. 3), with maximum intensity at ~161 °C, which allowed the first structural characterisation using Rietveld refinement (see above). At ~188 °C, diffraction from $Eu(BH_4)_2$ disappears possibly due to an amorphisation reaction.

At 265 °C, the onset of H_2 desorption occurs, along with an inflection in the PCT, TGA and DSC curves (Fig. 4). At the same temperature, the formation of a second crystalline compound is identified by SR-PXD, which may be a short lived intermediate, since its presence is only detected in a narrow temperature region from 267 to 304 °C (ΔT ~ 37 °C). During this temperature range, the TGA data indicates a mass loss of ~4.8 wt%, while upon the disappearance of this crystalline compound, a further 9.7 wt% is lost between 304 and 388 °C (Fig. 4a(i)). This indicates that the material is a hydrogen containing compound, while there is also a possibility for the inclusion of amorphous $LiBH_4$.[5] Indexing of this crystalline material allowed for the possibility of an orthorhombic or monoclinic crystal system and a variety of common borane polyhedra ($B_3H_8^-$, $B_6H_6^{2-}$, $B_{10}H_{10}^{2-}$, $B_{12}H_{12}^{2-}$) were investigated as prospective solutions. After Monte-Carlo optimisation using FOX,[34] no suitable structural models were identified.

At 310 °C, an emergence of a cubic phase with broad peaks is observed by SR-PXD. Rietveld analysis indicates that this is EuB_6 with a space group of $Pm\bar{3}m$ and a = 4.1100(6) Å at 430 °C. Hydrogen desorption is complete at ~420 °C according to MS data (Fig. 4a(iii)). This observed H_2 desorption is in accordance with the Sieverts data, which also indicates an inflection within this temperature range with a total pressure evolution corresponding to 6 wt% H_2 (Fig. 4b(i)).

The DSC data corroborates the events observed in the SR-PXD, TGA, MS and Sieverts data (Fig. 4a(ii)). The endothermic event at ~112 °C is indicative of the release of Me_2S from $Eu(BH_4)_2{\cdot}Me_2S$ but may also be attributed to the polymorphic phase transition of $LiBH_4$ from the low temperature orthorhombic phase to the high temperature hexagonal phase.[35, 36] The endothermic events at ~233, 294 and 366 °C support the observations noted above with regards to the thermal and decomposition reactions in the material, with the latter also being a potential decomposition of residual amorphous $LiBH_4$.

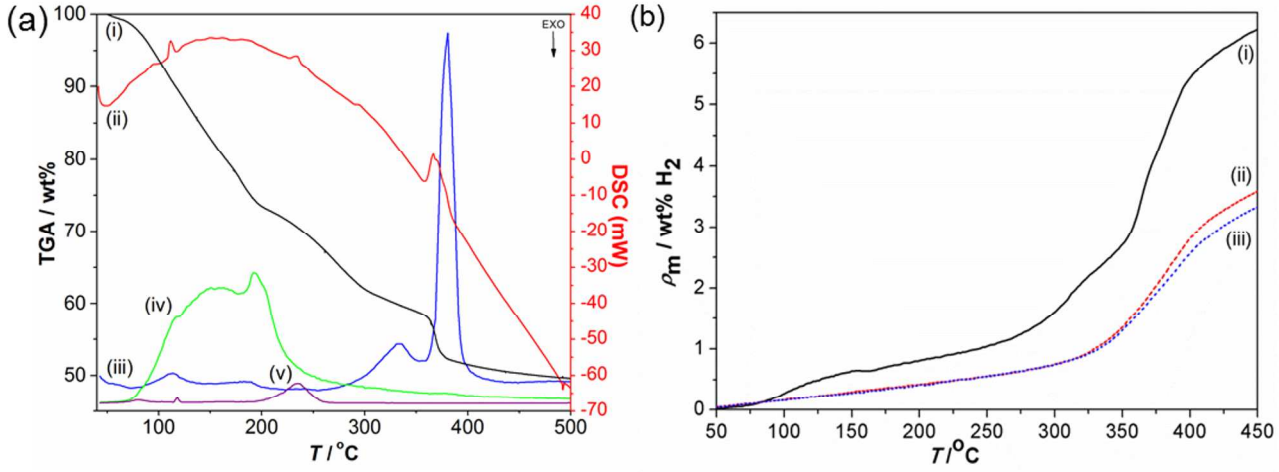

Fig. 4 (a) Thermal analysis of S1. (i) TGA, (ii) DSC, MS ((iii) H_2, (iv) Me_2S and (v) B_2H_6 qualitative desorption (B_2H_6 and Me_2S measurements multiplied by 20)) were measured simultaneously ($\Delta T/\Delta t$ = 5°C/min). (b) Three hydrogen desorptions ((i) first, (ii) second and (iii) third) measured by the Sieverts approach ($\Delta T/\Delta t$ = 3 °C/min, $p(H_2)$ = 1 bar). Hydrogen absorption were performed at 400 °C and $p(H_2)$ = 100 bar for 8 h.

Journal Name RSCPublishing

ARTICLE

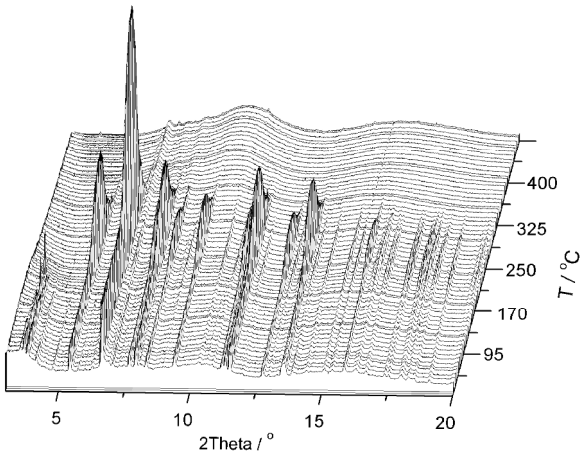

Fig. 5. *In situ* SR-PXD data for S4($\Delta T/\Delta t$ = 5 °C/min, λ = 0.5053 Å).

Thermal Decomposition of $SmCl_3$ + 3$LiBH_4$ (S4)

The thermal decomposition of S4 (Table 1) was observed by *in situ* SR-PXD and the results illustrated in Fig. 5. Initially, diffraction from $Sm(BH_4)_2$ along with a small quantity of a second compound are observed, and the latter may be an unidentified solvate, e.g. $Sm(BH_4)_2 \cdot xMe_2S$. The solvate is not as prominent in S4 as in S1, because S4 was annealed at 140 °C for 2 h after removal of the bulk solvent due to the product being a very sticky dark brown solid. The remainder of the solvent does not dissociate until the sample is heated above 165 °C. At this temperature, pure $Sm(BH_4)_2$ remains as the only diffracting compound in the sample and has maximum intensity at 225 °C (see diffraction pattern in Fig. 1b). The decomposition of $Sm(BH_4)_2$ is completed at ~335 °C, with no observable diffraction from SmB_6, as observed previously. The temperature of decomposition is higher than observed earlier, possibly due to the lack of halide impurities in the sample.[6]

The thermal analysis data measured by DSC, TGA and MS (Fig. E6†) corroborate the SR-PXD results. Since S4 was previously heated to 140 °C, gas desorption is not witnessed until after this temperature, at which point the remaining Me_2S dissociates along with some B_2H_6 and H_2. This culminates in a 10 wt% loss between 140 °C and 220 °C. The reason for the observance of B_2H_6 and H_2 at these temperatures is unclear, although the formation of B_2H_6 may follow from a continued reduction of Sm^{3+} which may still be present. A signal is not witnessed by DSC during this temperature range. The mass loss of 10 % measured by TGA is mainly attributed to the loss of solvent.

The onset of B_2H_6 desorption begins at ~175 °C, and has a maxima at 230 °C, and desorption is complete at ~360°C. The maxima also corresponds to the appearance of an endothermic signal in the DSC and also appears in the same region where $Sm(BH_4)_2$ has the greatest intensity in the PXD analysis. During this temperature range of 220 - 265 °C, an 11 wt% loss is also observed.

H_2 desorption begins at ~310 °C and has a maxima at ~330 °C. There is a corresponding DSC peak at 313 °C. TGA measurements also indicate a mass loss of ~5 wt% in the temperature region between 265 and 325 °C. This is the final decomposition of $Sm(BH_4)_2$ (theoretical gravimetric capacity 4.5 wt% H_2).

Sieverts measurements

The reversible hydrogen storage properties of $Eu(BH_4)_2$ (S1 and S3) were studied by Sieverts measurements in which the materials were cycled three times, revealing that partial reversibility is feasible (Figs. 4b and E4†). The first decomposition of S1 and S3 are very similar, with both indicating a two-step decomposition process. One major difference between desorption of S1 and S3 is the quantity of H_2 evolved. S1 releases over 6 wt%, whereas S3 only releases 2.5 wt% (gravimetrical H_2 content 4.4 wt%). This is due to the by-product contained in S3 (LiCl), which decreases the overall hydrogen content to 3.0 wt% (calculated for a sample with the ideal composition $Eu(BH_4)_2$-LiCl, 1:2), while the residual solvent contained in S1 contributes to the pressure evolution. S1 absorbs and then releases ~3.5 wt%, whereas S3 releases 1.25 wt%. In both samples, this desorption occurs in a one-step process with both starting at ~325 °C. The third dehydrogenation exhibits the same properties as the second cycle, with the same quantity of H_2 desorbed at the same temperatures for S1 and S3.

The material responsible for the 1.25 wt% reversible absorption exhibited by S3 is most likely EuH_2, which possesses a theoretical 1.31 wt% H. Unfortunately, EuH_2 is not observed by PXD after thermal treatment. The identity of the borane species after decomposition is also currently unknown, but is likely to be a highly stable species such as $B_{10}H_{10}^{2-}$ or $B_{12}H_{12}^{2-}$, as observed for $Mg(BH_4)_2$.[37] Alternatively, it could be the reversible hydrogenation of residual LiBH4.

Discussion

The products of the reaction between $EuCl_x$ and $x$$LiBH_4$ (x = 2, 3) produced by mechano-milling and wet chemistry techniques have shown some interesting similarities and differences. It appears that the synthesis of $Eu(BH_4)_2$ from $EuCl_3$ and $LiBH_4$ (S1) is facilitated by the reduction of the Eu^{3+} to Eu^{2+} by $LiBH_4$ dissolved in Et_2O, before extraction of the product $RE(BH_4)_2$ by Me_2S, resulting in a crystalline solvate. After desorption of the

solvent, the powder remains crystalline, which enables the diffraction pattern of $Eu(BH_4)_2$ to be collected (Fig. 3). This clarifies why $Eu(BH_4)_2$ was not observed after BM of $EuCl_3$ and $LiBH_4$ alone (S2), even after annealing,[6] while after extraction with Me_2S a reaction product was observed (detailed information for S2 and S3 are contained in the ESI†). Reduction to Eu^{2+} is a key process, as the milling of $EuCl_2$ with $LiBH_4$ (S3) yields $Eu(BH_4)_2$, although additional annealing promotes reaction completion and possibly crystallisation of the product (Fig. E5†). One peculiar upshot is the fact that after stirring in Me_2S, dissolution of S2 did not occur, although the reaction was complete. However, even though Me_2S addition did not dissolve $Eu(BH_4)_2$, it did crystallise the reaction products as observed in the *in situ* SR-PXD study of S2 (Fig. E1†). It is possible that the product after the initial reaction in Et_2O is an Et_2O adduct that is dissolvable in Me_2S. This would explain why Me_2S extraction of the ball milled sample was not possible.

The synthesis products and thermal desorption of $Sm(BH_4)_2$ (S4), prepared by solvent synthesis, contrasts the previously observed results for the sample prepared by BM.[6] Although S4 is allowed to stir in solvent for a longer time (two days compared to the five hours for milling), the reaction goes to completion and, as such, no crystalline starting materials are observed in the reaction product by PXD. The reduction of Sm^{3+} to Sm^{2+} by $LiBH_4$ in Et_2O may be the ultimate factor for the reaction, but the extraction from impurities in Me_2S enhances the purity and avoids any Cl^- substitution in $Sm(BH_4)_2$ to take place. The thermal decomposition of S4 has no crystalline intermediates besides the solvent phase and $Sm(BH_4)_2$. This situation is in total contrast to that observed in the sample of $SmCl_3$ with $6LiBH_4$ (BM), which initially contains α/β-$Sm(BH_4)_3$, $SmCl_3$ and some $LiSm(BH_4)_3Cl$.[6] During heating, α/β-$Sm(BH_4)_3$ is fully converted to $LiSm(BH_4)_3Cl$, which becomes $Sm(BH_4)_2$ above 200 °C.

The impurities significantly affect the decomposition temperature and mechanism of the divalent *RE* borohydride. The *in situ* SR-PXD measurement of S1 (Fig. 3) shows that after decomposition of $Eu(BH_4)_2$, an amorphous phase appears followed by an unidentified or new compound as an intermediate, before the appearance of EuB_6. In the two samples synthesised from $EuCl_3$ (S1 and S2), the appearance of $Eu(BH_4)_2$ is observed at ~105 °C, although the temperature range in which this compound is stable varies dramatically (Figs. 3 and E1†). Pure $Eu(BH_4)_2$ is stable up to 185 °C (S1), whereas the inclusion of impurities in the powder matrix promotes destabilisation and the temperature of amorphisation is reduced by 20 °C (S2). The majority of H_2 desorption is not found to occur after the disappearance of the crystalline $Eu(BH_4)_2$ phase but rather after 334 °C for the mixed material (S2 – Fig. E2†) and 350 °C for the pure material (S1, Fig. 4). This stimulates the notion for the formation of an intermediate phase before decomposition occurs, similar to the decomposition pathway of $Mg(BH_4)_2$.[37] This intermediate phase is prominent in the pure material, although the equivalent phase is not observed in the BM material. Destabilisation effects are also observed for $Sm(BH_4)_2$; S4 decomposes at 335 °C while impurities cause decomposition to occur at approximately 300 °C.[6] In comparison, these decomposition temperatures emulate the decomposition of the isostructural $Sr(BH_4)_2$, which decomposes at temperatures above 350 °C.[26]

The samples S1 and S3 show some reversibility with respect to hydrogen desorption and absorption (Figs. 4b and E4). EuH_2 is not observed by PXD after thermal treatment and the identity of the borane species is also currently unknown, but is likely to be highly stable as observed for $Mg(BH_4)_2$.[37] However, EuB_6 was observed in the *in situ* SR-PXD study. A similar situation was previously observed for $LiCe(BH_4)_3Cl$, where partial reversibility was observed and was attributed to CeH_2.[2] Mixed phases ultimately reduce the hydrogen capacity of these materials and inhibit the reversible hydrogenation of these borohydrides due to the formation of side products. Another factor that affects the reversibility of the material is the evolution of B_2H_6 during decomposition, as observed by MS analysis. The higher gas release recorded for S1 may also be due to remaining $LiBH_4$ from the initial synthesis, which subsequently decomposes during desorption cycles 2 and 3, although the lack of impurities in S1 may allow a greater chance that some degree of reformation is achievable.

Conclusions

$Eu(BH_4)_2$ and $Sm(BH_4)_2$ have been prepared free from solvents and LiCl impurities for the first time. The crystal structures have been solved by Rietveld refinement of SR-PXD data with both compounds crystallising in the orthorhombic space group *Pbcn* (no. 60). The structures differ only by an increase in unit cell parameters and bond distances according to the change in ionic radii of the *RE* metal centre. The structures of both *RE* metal borohydrides can be described by *RE*-$(BH_4)_6$ octahedra sharing edges with two other octahedra, thus building chains in the *c*-direction (Fig. 2). Each BH_4^- unit is surrounded by three Eu atoms in a distorted trigonal planar environment.

This work provides a new synthesis route to obtain pure $Eu(BH_4)_2$ and $Sm(BH_4)_2$. The synthesis is based on the reduction of the *RE* metals from +3 to +2 oxidation states by $LiBH_4$ in Et_2O solvent, followed by extraction in Me_2S, which also coordinates to the *RE* metals, forming a crystalline solvate as product.

The decomposition pathway of both materials has been extensively studied by *in situ* SR-PXD, TGA, DSC, TPD and PCT measurements and compared against equivalent materials prepared by mechano-milling. The inclusion of LiCl impurities in the powder matrix destabilizes the *RE*$(BH_4)_2$ complex and promotes the onset of decomposition to occur at least 20 °C lower than the pure material.

The reversible hydrogenation of the pure and mechano-milled $Eu(BH_4)_2$ samples were measured by PCT analysis and revealed that up to ~3.5 wt% is reversibly absorbed over three cycles of the pure material, while the mechano-milled material reversibly absorbs ~1.25 wt%.

The fact that these $RE(BH_4)_2$ compounds can now be synthesised in high purity allows further investigations to be conducted. Future work on these materials will likely divulge the ionic conductivity, magnetic and photoluminescence properties.

Acknowledgements

We would like to thank the project teams at the Swiss Norwegian Beam Line (SNBL) at the European Synchrotron Research Facility (ESRF), Grenoble, France; Petra, Germany and MAXLab, Sweden. Financial support is acknowledged from The Research Council of Norway through the FRIENERGI and SYNKNØYT programs. We also thank Jørn Eirik Olsen for the preparation of sample S2. The work was supported by the Danish National Research Foundation, Centre for Materials Crystallography (DNRF93), the Danish Council for Strategic Research via the research project HyFillFast, and the Danish Research Council for Nature and Universe (Danscatt). We are grateful to the Carlsberg Foundation.

Notes and references

[a] Physics Department, Institute for Energy Technology, P.O. Box 40, NO-2027, Kjeller, Norway. Fax: +47 63 81 09 20; Tel: +47 97 40 88 44; E-mail: bjorn.hauback@ife.no
[b] WPI-Advanced Institute for Materials Research, Tohoku University, 2-1-1 Katahira, Aoba-ku, Sendai 980-8577, Japan. E-mail: terry_humphries81@hotmail.com.
[c] Centre for Materials Crystallography (CMC), Interdisciplinary Nanoscience Center (iNANO) and Department of Chemistry, University of Aarhus, Langelandsgade 140, DK-8000 Århus C, Denmark. Fax: +45 8619 6199; Tel.: +45 8942 3894; E-mail: trj@chem.au.dk.

† Electronic Supplementary Information (ESI) available: Experimental syntheses of S1-4; thermal decomposition data and interpretation for sample S2 including in situ XRD, TGA-MS, data; thermal decomposition data for sample S3 including in-situ and ex-situ XRD and PCT data; FT-IR spectroscopy data and interpretation for samples S1-4. See DOI: 10.1039/b000000x/

1. M. B. Ley, L. H. Jepsen, Y.-S. Lee, Y. W. Cho, J. B. v. Colbe, M. Dornheim, M. Rokni, J. O. Jensen, M. Sloth, Y. Filinchuk, J. E. Jørgensen, F. Besenbacher and T. R. Jensen, *Mater. Today*, 2014, **17**, 122-128.
2. C. Frommen, M. H. Sørby, P. Ravindran, P. Vajeeston, H. Fjellvåg and B. C. Hauback, *J. Phys. Chem. C*, 2011, **115**, 23591-23602.
3. J. E. Olsen, C. Frommen, M. H. Sørby and B. C. Hauback, *RSC Adv.*, 2013, **3**, 10764-10774.
4. M. B. Ley, S. Boulineau, R. Janot, Y. Filinchuk and T. R. Jensen, *J. Phys. Chem. C*, 2012, **116**, 21267-21276.
5. M. B. Ley, D. B. Ravnsbæk, Y. Filinchuk, Y. S. Lee, R. Janot, Y. W. Cho, J. Skibsted and T. R. Jensen, *Chem. Mater.*, 2012, **24**, 1654-1663.
6. J. E. Olsen, C. Frommen, T. R. Jensen, M. D. Riktor, M. H. Sørby and B. C. Hauback, *RSC Adv.*, 2013, **4**, 1570-1582.
7. F. C. Gennari, *J. Alloys Compd.*, 2013, **581**, 192-195.
8. H. W. Li, Y. G. Yan, S. Orimo, A. Züttel and C. M. Jensen, *Energies*, 2011, **4**, 185-214.
9. C. Frommen, N. Aliouane, S. Deledda, J. E. Fonneløp, H. Grove, K. Lieutenant, I. Llamas-Jansa, S. Sartori, M. H. Sørby and B. C. Hauback, *J. Alloys Compd.*, 2010, **496**, 710-716.
10. D. B. Ravnsbæk, Y. Filinchuk, R. Cerny, M. B. Ley, D. r. Haase, H. J. Jakobsen, J. Skibsted and T. R. Jensen, *Inorg. Chem.*, 2010, **49**, 3801-3809.
11. A. Remhof, A. Borgschulte, O. Friedrichs, P. Mauron, Y. Yan and A. Züttel, *Scr. Mater.*, 2012, **66**, 280-283.
12. C. W. Thiel and R. L. Cone, *J. Lumin.*, 2011, **131**, 386-395.
13. C. Eylem, G. Saghiszabo, B. H. Chen, B. Eichhorn, J. L. Peng, R. Greene, L. Salamancariba and S. Nahm, *Chem. Mater.*, 1992, **4**, 1038-1046.
14. L. J. Shawklein, T. K. Hatwar, S. J. Burns, S. D. Jacobs and J. C. Lambropoulos, *J. Mater. Res.*, 1992, **7**, 329-334.
15. A. Unemoto, M. Matsuo and S. Orimo, *Adv. Funct. Mater.*, 2014, **24**, 2267-2279.
16. J. Huot, D. B. Ravnsbæk, Z. F. Cuevas, M. Latroche and T. R. Jensen, *Prog. Mater. Sci.*, 2013, **58**, 30-75.
17. R. Cerny, G. Severa, D. B. Ravnsbæk, Y. Filinchuk, V. D'Anna, H. Hagemann, D. Haase, C. M. Jensen and T. R. Jensen, *J. Phys. Chem. C*, 2010, **114**, 1357-1364.
18. J. E. Olsen, M. H. Sørby and B. C. Hauback, *J. Alloys Compd.*, 2011, **509**, L228-L231.
19. B. D. James, *Record of Chemical Progress*, 1970, **31**, 199-&.
20. E. R. Bernstein and K. M. Chen, *Chem. Phys.*, 1975, **10**, 215-228.
21. S. Marks, J. G. Heck, M. H. Habicht, P. Oña-Burgos, C. Feldmann and P. W. Roesky, *J. Am. Chem. Soc.*, 2012, **134**, 16983-16986.
22. H. Hagemann and R. Cerny, *Dalton Trans.*, 2010, **39**, 6006-6012.
23. T. R. Jensen, T. K. Nielsen, Y. Filinchuk, J.-E. Jørgensen, Y. Cerenius, E. M. Gray and C. J. Webb, *J. Appl. Crystallogr.*, 2010, **43**, 1456-1463.
24. S. Vogel, L. Ehm, K. Knorr and C. Braun, *Adv. X-Ray Anal.*, 2002, **45**, 31-33.
25. A. P. Hammersley, *Fit2D: An introduction and Overview; ESRF Internal Report.*, 1997.
26. D. B. Ravnsbæk, E. A. Nickels, R. Cerny, C. H. Olesen, W. I. F. David, P. P. Edwards, Y. Filinchuk and T. R. Jensen, *Inorg. Chem.*, 2013, **52**, 10877-10885.
27. A. Boultif and D. Louer, *J. Appl. Crystallogr.*, 2004, **37**, 724-731.
28. A. C. Larson and R. B. Von Dreele, *Los Alamos National Laboratory Report LAUR*, 2000, 86-748.
29. B. H. Toby, *J. Appl. Crystallogr.*, 2001, **34**, 210-213.
30. K. J. Gross and B. Hardy, Recommended Best Practices for Characterizing Engineering Properties of Hydrogen Storage Materials, http://www1.eere.energy.gov/hydrogenandfuelcells/pdfs/best_practices_hydrogen_storage_section_6.pdf, Accessed 06/12/2014.
31. PCTPro 2000 - Calorimetry and thermal analysis, http://www.setaram.com/PCTPro.htm, Accessed 06/12/2014.
32. A. Boultif and D. Louer, *J. Appl. Crystallogr.*, 1991, **24**, 987.
33. M. B. Ley, M. Paskevicius, P. Schouwink, B. Richter, D. A. Sheppard, C. E. Buckley and T. R. Jensen, *Dalton Trans.*, 2014, **43**, 13333-13342.
34. V. Favre-Nicolin and R. Cerny, *J. Appl. Crystallogr.*, 2002, **35**, 734-743.

35. A. Züttel, P. Wenger, S. Rentsch, P. Sudan, P. Mauron and C. Emmenegger, *J. Power Sources*, 2003, **118**, 1-7.
36. J. P. Soulié, G. Renaudin, R. Černý and K. Yvon, *J. Alloys Compd.*, 2002, **346**, 200-205.
37. C. Pistidda, S. Garroni, F. Dolci, E. G. Bardají, A. Khandelwal, P. Nolis, M. Dornheim, R. Gosalawit, T. Jensen, Y. Cerenius, S. Suriñach, M. D. Baró, W. Lohstroh and M. Fichtner, *J. Alloys Compd.*, 2010, **508**, 212-215.

Synthesis of halide free $RE(BH_4)_2$ (RE = Eu, Sm) complexes are detailed. Their crystal structures have been determined and thermal decomposition pathways studied by *in-situ* SR-PXD and thermal analysis techniques.